Available online at www.sciencedirect.com
ScienceDirect
Journal of Photochemistry and Photobiology A: Chemistry 189 (2007) 105–113
Journal of Photochemistry and Photobiology A:Chemistry
www.elsevier.com/locate/jphotochem

Formation of 3,4,9,10-perylenetetracarboxylicdianhydride nanoparticles with perylene and polyyne byproducts by 355 nm nanosecond pulsed laser ablation of microcrystal suspensions

Jonathan Hobley [a,*], Taro Nakamori [b], Shinji Kajimoto [b], Motohiro Kasuya [b], Koji Hatanaka [b], Hiroshi Fukumura [b], Satoru Nishio [c,✠]

[a] *Institute of Materials Research and Engineering (IMRE), 3 Research Link, 117602 Singapore*
[b] *Department of Chemistry, Graduate School of Science, Tohoku University, Aoba-ku, Sendai 980-8578, Japan*
[c] *Department of Applied Chemistry, Faculty of Science and Engineering, Ritsumeikan University, 1-1-1, Noji-Higashi, Kusatsu, Shiga 525-8577, Japan*

Received 14 August 2006; received in revised form 14 December 2006; accepted 17 January 2007
Available online 21 January 2007

Abstract

Nanoparticles of the insoluble organic compound 3,4,9,10-perylenetetracarboxylicdianhydride were prepared by nanosecond pulsed laser irradiation of microcrystalline solid suspensions in polar solvents using the 3rd harmonic (355 nm) from a Nd:YAG laser. The initially cloudy suspensions became transparent clear red dispersions that passed through a 0.2 μm membrane filter 1 day after 30 min of irradiation at laser fluences greater than 130 mJ cm^{-2}. Filtering reduced the red color indicating that it originated from light absorption by particles or aggregates with a size range spanning the 0.2 μm filter cut-off. This is consistent with scanning electron microscope images. Whether or not the particles passed through the filter depended on how long they were aged. Initially formed dispersions did not pass through, whereas those which had been aged for several hours did, indicating that the nanoparticles were aggregated and that the aggregate size depended on the standing time after laser irradiation. HPLC analysis revealed perylene and C_8, C_{10}, C_{12}, C_{14} polyynes byproducts, which probably formed respectively in a 3 photon photochemical and a photothermal processes at the surface of the PTCDA particles. Initially the perylene production rate was rapid, but as the PTCDA particles' surface became decomposed it slowed down. However, it increased again as the surface area of the PTCDA particles became larger as smaller nanoparticles formed and after the thermal decomposition of the surface was quenched. When the particles became smaller the thermal processes were quenched and polyyne production stopped.

Keywords: Nanoparticle; Laser ablation; 3,4,9,10-perylenetetracarboxylicdianhydride; PTCDA

1. Introduction

3,4,9,10-Perylenetetracarboxylicdianhydride (PTCDA structure shown in Scheme 1) and compounds such as 3,4,9,10-perylenetetracarboxylicdiimide (PTCDI) are important candidate materials for organic semi-conductors due to their extremely close π–stacking in the solid state.

Some of these compounds have even been used in electron transfer layers of organic electro luminescent devices [1,2]. Among these compounds, PTCDA is considered to be the archetype for organic semi-conductive materials. It is also important as a starting material in the synthesis of various kinds of organic compounds, including the low dimensional conducting polymer called polyperinaphthalene (PPN) which is thought to be formed by elimination of the anhydride groups from PTCDA [3,4]. To date various methods have been proposed for enhancing the elimination of the anhydride side groups in order to enhance PPN production, however, the exact elimination mechanism is still not clear [5–10].

If PTCDA-related organic semi-conductive materials can be made into thin-films, then these films can be components in

* Corresponding author. Tel.: +65 6874 1483; fax: +65 6872 0785.
E-mail address: hobleyj@imre.a-star.edu.sg (J. Hobley).
✠ We regret that Satoru Nishio who initiated and guided this work began a long battle with illness during its progress. He passed away on 15th October 2006. Our deepest sympathy goes to his wife and his two sons.

1010-6030/$ – see front matter © 2007 Elsevier B.V. All rights reserved.
doi:10.1016/j.jphotochem.2007.01.016

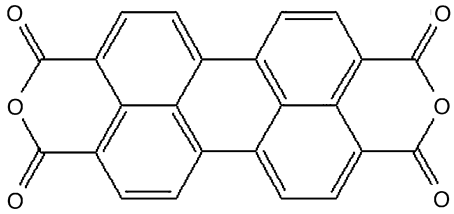

Scheme 1.

functional devices. However, since PTCDA has very low solubility in all but the most aggressive solvents, almost all of the currently available methods of manipulation are dry processes [1,2,11–16]. For large scale or ambient laboratory processing wet techniques are sometimes preferable to dry ones when taking into consideration cost performance, versatility and the ease of preparing thin films. For example, it is possible to create coatings from nanoparticles that have been dispersed in a solvent by spreading the dispersion on the required substrate and then evaporating the solvent. It is therefore desirable to find alternative methods for dispersal of PTCDA and similar compounds to allow easy handling for larger scale production techniques.

Nanoparticle formation has recently attracted a great deal of interest due to the possibility of tailoring the specific material function depending on the particle size. In relation to this there is one advantage of PTCDA's low solubility, since the availability of a poor solvent is the first requirement for the formation of organic nanoparticles by either rapid precipitation methods [17–20] or ablative methods [21–29]. The former method requires that the material to be made into nanoparticles is first dissolved in a good solvent and this solution is then rapidly quenched into an unstable region of its phase diagram by fast injection into a poor solvent, which results in precipitation of nano-crystals. However, this method cannot be applied to PTCDA and its related compounds as they do not have a good solvent. This means that ablation is the only viable method of causing particle division to create nanoparticles.

The formation of nanoparticles by laser ablation in the liquid phase has recently become popular, not only for the preparation of various metal and metal-oxide nanoparticles [21–26], but also for making nanoparticles of organic materials from solid suspensions in poor solvents [27–29]. For example, Asahi et al., prepared nanoparticles of vanadyl phthalocyanine (VOPc) by laser ablation of VOPc powders, which were dispersed in water, using a 351 nm pulsed excimer laser.

When ablating organic suspensions in the liquid phase it is often possible to isolate novel products. For example, polyyne has been prepared by laser ablation of graphitic materials in the liquid phase [30–31]. As mentioned previously, it has been reported that laser ablation of PTCDA solid in a vacuum results in the loss of its anhydride side groups leading to the formation of perylene based polymeric structures such as PPN [5–8,32]. In the present study it was therefore also interesting, from a mechanistic point of view, to try to observe the production of soluble side products resulting from laser ablation of PTCDA suspensions.

In this study, PTCDA nanoparticle formation was attempted, using laser ablation with the third harmonic of a Nd:YAG laser, in various solvents in which the PTCDA was insoluble. It was found that PTCDA nanoparticles formed in polar solvents but not in non-polar solvents. In addition, it was found that a photothermal reaction occurred resulting in the formation of four polyynes (C_8H_2, $C_{10}H_2$, $C_{12}H_2$ and $C_{14}H_2$) and that a multiphoton photochemical reaction occurred that resulted in the formation of perylene. The mechanism of formation for these compounds will be discussed.

2. Experimental

2.1. Materials and apparatus

A schematic representation of the apparatus used for laser ablation of PTCDA suspensions is shown in Fig. 1. 0.2 mg cm^{-3} of PTCDA powder (Aldrich Chemicals) was dispersed in 99.5% pure fluorimetric grade ethanol (Cica Reagents) water (distilled) DMSO (Wako Chemicals) cyclohexane (Wako Chemicals) or toluene (Wako Chemicals). The PTCDA and all solvents employed were used as received.

Laser ablation of 10 cm^3 of the PTCDA suspensions was achieved using the 3rd harmonic (355 nm) from a Spectra Physics CGR 230 Nd:YAG laser, with an 8 ns pulse duration, operating at 10 Hz (unless otherwise stated). The laser fluence used was in the range from 0 to 200 mJ cm^{-2} $pulse^{-1}$. The spot size was determined to be circular and to have an area of 0.5 cm^2 using burn paper. The laser power was measured with an Ophir Optronics power meter. The unfocussed laser light was directed into a glass cell containing the suspensions of PTCDA in different solvents. The suspensions were magnetically stirred in order to achieve more even irradiation of the cell contents during the ablation period. As a note on safety, it is important that the interface between the air and a flammable organic liquid is not irradiated by a high fluence nanosecond laser pulse as this may ignite the liquid. Further the vessel containing the liquid

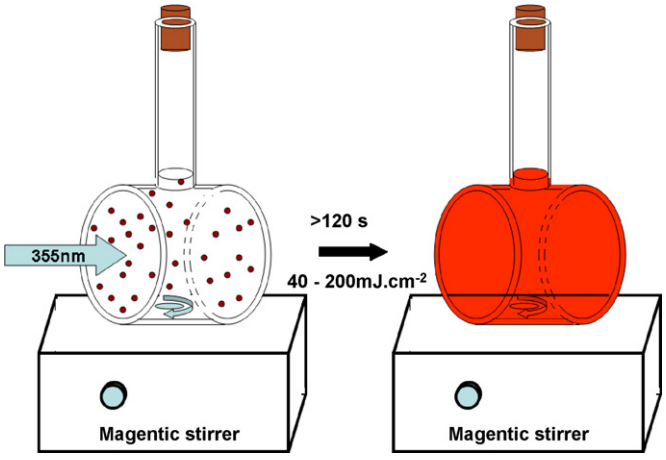

Fig. 1. Schematic representation of the apparatus used for the formation of PTCDA nano-particles by laser ablation of a 0.2 mg/cm^3 suspension of PTCDA in 10 cm^3 of "poor" solvent in a cell of 1.5 cm path length and diameter of 3 cm.

should be sealed to prevent ignition via vapors, in the event of dust entering the laser beam path.

2.2. Monitoring nanoparticle formation

At various times after the start of the cumulative ablation process, UV–vis absorption spectra of stirred unfiltered PTCDA solutions were measured off-line using a Shimadzu UV 1600-PC UV-visible absorption spectrometer. The absorption spectra of the solutions of PTCDA nanoparticles were measured in transmission mode and could be compared to those of solvated PTCDA measured in transmission mode in DMSO and solid pellets of PTCDA measured in diffuse reflectance mode. The formation of nanoparticles was initially assessed by whether or not the solution became a transparent with a typical solid PTCDA absorption spectrum with a low baseline in the UV–vis region indicating low levels of light scattering. However, the PTCDA nanoparticles could also be directly observed, after filtration (0.2 μm Whatman, syringe type, PTFE, Puradisc, 25TF, filters) on the filter, or after evaporation onto microscope cover slides, using an S-4500 Hitachi scanning electron microscope.

2.3. Monitoring the formation of by-products

To monitor the formation of by-products during nanoparticle production the ablated solutions were first filtered, using 0.2 μm Puradisc 25TF filters, immediately after the irradiation had been stopped. Fluorescence excitation and emission measurements were made on these filtered ablated mixtures using an F-4500 Hitachi emission spectrometer in order to determine the perylene derivative production as a function of irradiation time and laser fluence. The irradiation time for the determination of the fluence dependence of perylene production was 20 min.

UV–vis absorption spectra on similarly filtered samples were measured in order to evaluate the polyyne yield as a function of laser ablation time and fluence (20 min irradiation time). HPLC analysis was carried out on the filtrates using a Hitachi L 6000 pump with an L 4000 UV–vis detector in order to identify which polyyne compounds formed during ablation. The column was reverse phase Inertsil (Tm) ODS-2 from GLS Science and the solvent was a 50:50 mixture of water (distilled) and HPLC grade acetonitrile (Cica Reagents).

Emission spectra of stirred PTCDA solutions were measured in situ, using an IMUC multi-channel-plate (MCP) detector, during manually triggered shot by shot laser excitation, in order to investigate the shot to shot evolution of the emission spectra of the suspensions.

3. Results and discussion

3.1. Formation of PTCDA nanoparticles

Stable PTCDA nanoparticles, having a size less than 200 nm, formed after laser ablation in polar solvents such as water and ethanol, but they did not form in non-polar solvents such as cyclohexane and toluene. This may be because the nanoparticles require polar interactions in order to stabilize them and prevent re-aggregation. The following criteria were used to establish whether stable nanoparticles (<200 nm) form or not.

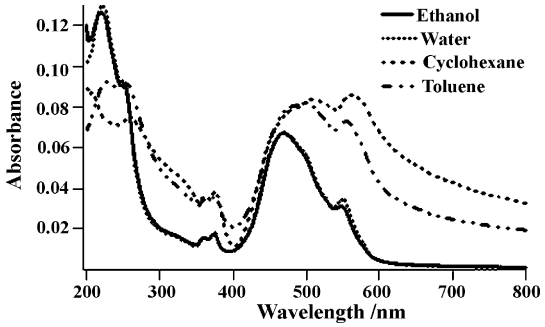

Fig. 2. Spectra obtained for unfiltered samples after laser ablation of PTCDA suspensions in various solvents (200 mJ cm^{-2} 20 min).

(1) Firstly we assessed whether the absorption spectrum of the suspension achieved a low baseline in the long wavelength region at 750 nm or above. If it did not then the suspension was assessed to be highly scattering and made up of particles that were larger than or of the order of the wavelength of light (See Fig. 2). This test was also confirmed by eye in that the suspension could be classified as cloudy or clear, since absorption at long wavelength could also be due to new phases of the PTCDA.
(2) Secondly the suspensions were passed through 0.2 μm membrane filters at various times after ablation. If no red color passed through the membrane then the particles were surely greater than 200 nm in size.
(3) Thirdly, the suspensions were coarse filtered with a Whatman filter paper to remove large particulate matter and the slightly cloudy supernatant was allowed to stand for a period of 1 week during which time it was visually inspected. If the solid matter all settled and no red color remained in the supernatant then it was assumed that the cloudy dispersion had been unstable and/or was made up of particles that were large enough to be affected by gravity.

Using these tests the polar solvents, water and ethanol were concluded to be effective for the production of nanoparticles smaller than 200 nm in size and the non-polar solvents, toluene and cyclohexane were concluded to be ineffective for the production of nanoparticles smaller than 200 nm in size. The toluene and cyclohexane dispersions remained visually scattering to the eye. Despite this it is clear from Fig. 2 that even in these non-polar solvents the spectral features of PTCDA were clearly seen. Further, it is possible that the long tail to the absorption above 600 nm is contributed to by absorption by trapped low energy absorption CT sizes within the lattice. Long tails to the CT absorption have been observed under certain conditions of PTCDA film growth and these were attributed to different orientations within the lattice [34]. Division and re-aggregation in the non-polar solvents may well result in inhomogeneity within the aggregates leading to an increase in trap sites. We propose that in the non-polar solvents the long tail is caused by the scattering that is evident to the eye, but is probably also contributed

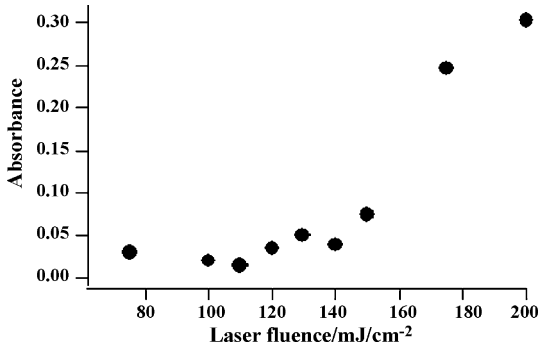

Fig. 3. Fluence dependence of the PTCDA absorbance at 464 nm for samples filtered through a 0.2 μm filter 1 day after 30 min of irradiation.

to by increased inhomogeneity and trapped CT sites within the aggregated particles.

In the polar solvents, only ablation above a threshold fluence of around 130 mJ cm^{-2} resulted in the formation of high yields of nanoparticles below 200 nm in size, as determined by filtration through a 0.2 μm filter 1 day after ablation for 30 min (Fig. 3). However, at fluences below this the suspensions did become transparent red dispersions and some trace red color did pass through the filter. On the other hand, in the absence of ablation the same result could not be obtained by other dispersal means. Even extended periods of sonication did not result in dispersion of the PTCDA into the solution and the suspension always remained cloudy. No PTCDA passed through a 0.2 μm filter even after extended periods of sonication. The significance of this threshold is probably that, at a given fluence, there is a minimum size of particle that can be obtained and that for a minimum size of 200 nm the required fluence is ∼130 mJ cm^{-2}. If the filter size were 100 nm then the threshold fluence to pass through the filter would probably be higher. Pyatenko et al., describe that photothermal division of particles critically depends on both the laser fluence and the particle size [35].

SEM images of PTCDA nanoparticles that were produced after irradiation at a fluence of 200 mJ cm^{-2}, using different irradiation times, are shown in Fig. 4. As shown in Fig. 4(a) after 2 min large particles of nearly 200 nm in size had formed. The surface of these larger particles appeared broken and fractured. After irradiation for 20 min smaller nanoparticles had formed as seen in Fig. 4(b), however, on the glass cover slide these formed larger aggregates. These aggregates may also exist in the solution as suggested from absorption spectra of filtrates described later. The dispersed nanoparticles formed at longer irradiation times were powder like and they were too small to determine weather they were amorphous or if they had some crystalline form. For comparison the needle type micro-crystals of the initial PTCDA powder are shown in Fig. 4(c). The filtered particles could also be observed on the membrane filter as shown in Fig. 4(d). These filtered particles were only a few hundred nanometers in size.

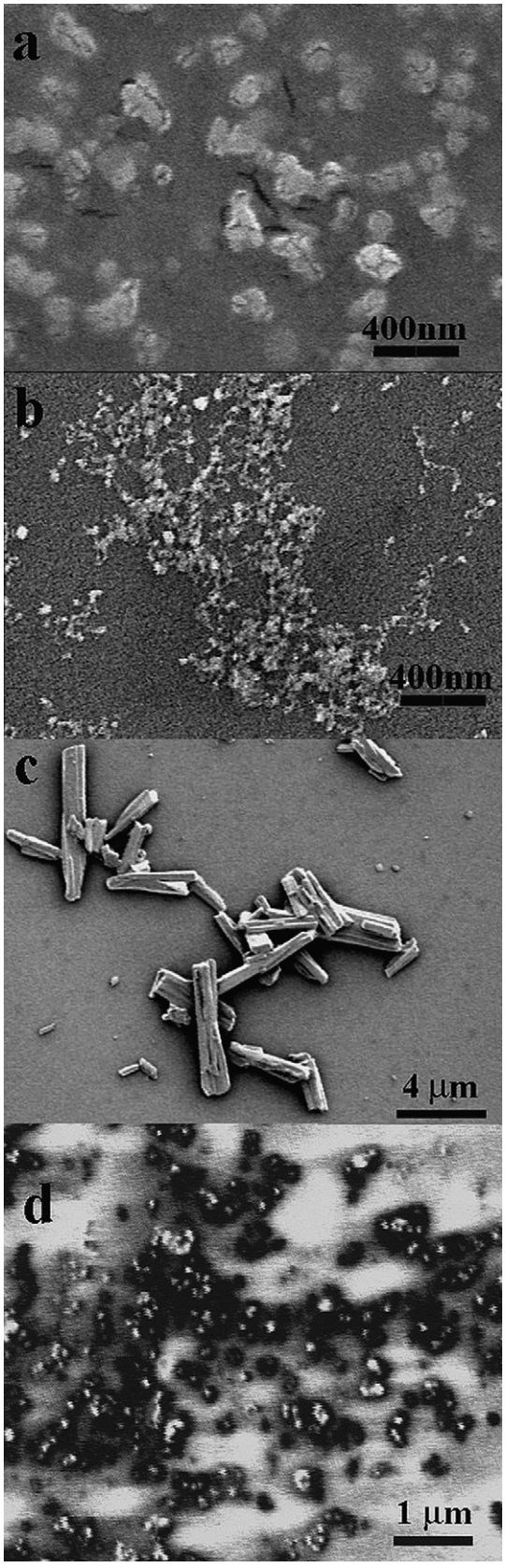

Fig. 4. SEM images of particles formed by ablation at 10 Hz with a fluence of 200 mJ cm^{-2} (a) Nanoparticles formed after 2 min of irradiation. (b) After 20 min of irradiation. (c) The starting material after sonication. (d) PTCDA nano-particles on a 0.2 μm membrane filter after extraction from ethanol.

3.2. Spectra of PTCDA nanopaticles

The solubility of PTCDA was found to be very limited in all solvents used except DMSO. The absorption spectrum obtained

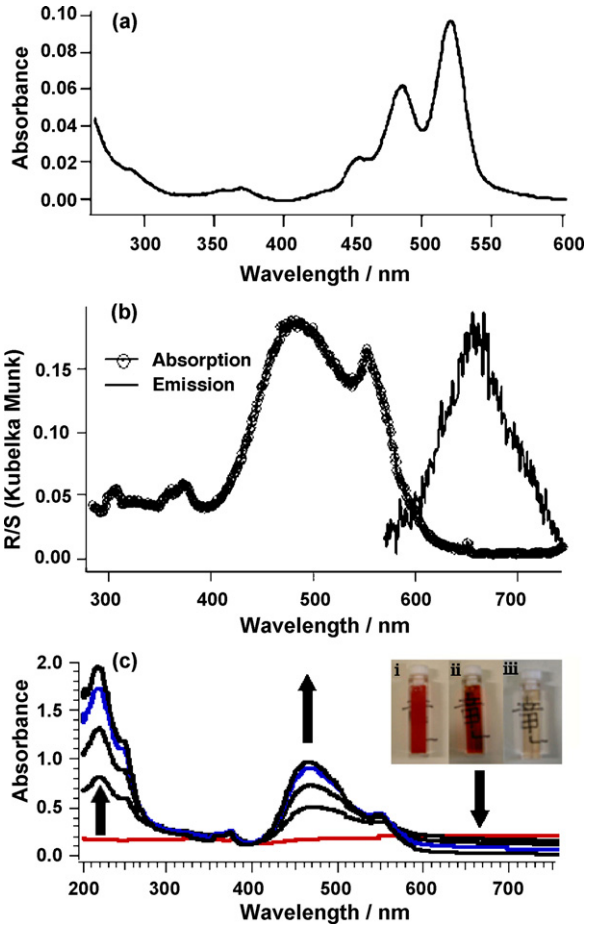

Fig. 5. (a) Absorption spectrum of PTCDA in DMSO. (b) Diffuse reflectance and emission spectrum of a PTCDA pellet. (c) Absorption spectra of a PTCDA suspensions in ethanol at different irradiation times (0, 0.5, 1, 1.5, 2 min) during ablation with a pulse fluence of 150 mJ cm^{-2}. Inset: photographs of the PTCDA suspentions. (i) The starting material; (ii) just after irradiation—unfiltered; (iii) a few hours after irradiation–filtered).

for the DMSO solution is shown in Fig. 5(a). This can be compared to the spectrum of solid PTCDA that was measured in diffuse reflectance mode, which is shown in Fig. 5(b). Clear differences are apparent between the solid's diffuse reflectance spectrum and the solution's absorption spectrum. The solution's absorption spectrum has clear vibrational structure, whereas in the solid the vibrational structure is lost and a new CT band is observed at longer wavelength, which has its origin in the π-stacking of the PTCDA in the solid state. The ratio of CT to singlet–singlet absorption for the solid diffuse reflectance spectrum is similar to previously reported absorption spectra measured in transmission mode [15]. The PTCDA emission at around 650 nm appears to originate from the CT band in the solid.

The evolution of the absorption spectra of unfiltered PTCDA samples, during nanoparticle production by laser ablation, is shown in Fig. 5(c). The initial absorption spectrum before ablation has a raised baseline with weak features that are consistent with the diffuse reflection spectrum of solid PTCDA. This spectrum results from light scattering by the large PTCDA solid micro-crystals, and the weak PTCDA absorption features are present due to diffuse reflections and surface absorption in this scattering medium. During the ablation process this baseline dropped as the particle size diminished and an absorption spectrum was obtained that was similar, but not identical to, a typical solid PTCDA diffuse reflectance spectrum. The most notable difference between the solid diffuse reflectance spectrum, the absorption spectra from the literature [15] and the nanoparticle's absorption spectrum, was the reduced ratio of the CT to singlet–singlet absorption bands in the nanoparticle's absorption spectrum. Similar absorption spectra to the nanoparticle's absorption spectra have been reported for deposited films [16]. In this previous report it was found that PTCDA films grown at room temperature had smaller grain size than those formed at higher temperature and that the room temperature film also had an absorption spectrum in which the CT to singlet–singlet band ratio was lower than when the film was made at higher temperature. Hence, the CT to singlet–singlet band ratio seems to be dependent on the particle size. The current observation, that the CT to singlet–singlet band ratio is different for microcrystals and nanoparticles, is consistent with this result.

In the inset of Fig. 5(c) solutions before and after irradiation are shown. Also the nanoparticle dispersion after filtration, just after ablation was stopped, is shown. From this it is clear that the initially cloudy suspension became a non-scattering dispersion of particles.

From Fig. 6 inset it can also be seen that just after the cessation of the ablation process, it was still possible to remove almost all of the PTCDA nanoparticles from the solution by filtration with a 0.2 μm membrane filter. The amount of PTCDA passing through the filter increased with standing time, reaching a peak after several hours. This finding indicates that, just after ablation, the nanoparticles are held together, as larger aggregates, by an attractive force and that this force diminishes with time. In the absence of other rational explanations, we suggest that mechanical cleavage of the PTCDA particles during ablation may have left some residual static electrical charge on the particles. If this occurred then the particles may form loose aggregates, which cannot pass through the filter. These loose aggregates may then disperse to smaller ones with time as the static charge decays. The absorbance due to PTCDA in solutions which had passed through the 0.2 μm membrane filter was always less than the unfiltered dispersion, indicating that particles or extended aggregates of varying size formed and that some of these were smaller than 200 nm in diameter, whereas others were larger. This find-

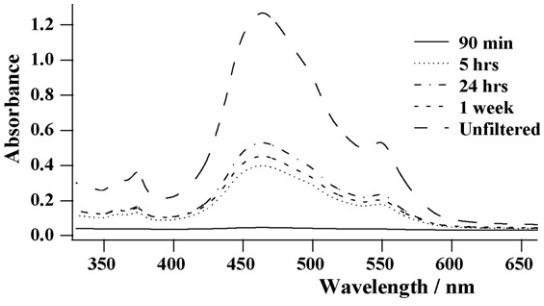

Fig. 6. Spectra of unfiltered nanoparticles compared to suspensions filtered at different times after the cessation of irradiation (150 mJ/cm^2, 20 min).

Table 1
Peak positions assigned to the polyynes C_8H_2, $C_{10}H_2$ and $C_{12}H_2$ using HPLC together with the values reported in the literature

Reference	C_8H_2 (13.8 min)	$C_{10}H_2$ (45.8 min)	$C_{12}H_2$ (–)	$C_{14}H_2$ (–)
Our data	216, 225 nm	228, 239, 252 nm	262, 277 nm	297 nm
Tsuji et al.[a]	215, 225 nm	228, 238, 251 nm	248, 259, 273 nm	295 nm
Eastmond et al.[b]	216, 226 nm	228, 239, 252 nm	248, 261, 275 nm	297 nm

[a] From [32].
[b] From [33].

ing may be important in explaining why non-polar solvents were not good for nanoparticle (<200 nm) formation, since any static charge would dissipate much more slowly in solvents with a low dielectric constant and permanent re-aggregation to form stable larger aggregates may be favored over de-aggregation to form stable nanoparticles.

When the dispersions were left to stand for longer periods the amount of PTCDA passing through the filter again diminished. In many cases the PTCDA re-precipitated after several weeks of standing time. This indicates a long-term aging effect results in re-aggregation.

3.3. UV absorption spectra of polyynes formed in the filtrate

The near colorless filtrates obtained after 0.2 μm filtration, just after the ablation had stopped, were analyzed using UV-absorption spectroscopy. The absorption spectra obtained are shown in Fig. 7(a) along with the peak assignments. These UV-absorption spectra had several sharp peaks and the intensity of these peaks increased with longer laser irradiation times or higher laser fluences. The origin of these peaks was assigned to the polyynes C_8H_2, $C_{10}H_2$, $C_{12}H_2$ and $C_{14}H_2$ using either HPLC or by the peak position in the spectrum or by both of these tests. The elution times and absorption peak positions were compared to data previously reported by Tsuji et al. [31] A comparison of the current data with that in the literature, for the spectral peak positions and the HPLC elution times, is given in Table 1.

Tsuji et al. obtained C_nH_2 ($n = 8$, 10, 12, 14, 16) after laser ablation of graphite in benzene, toluene and hexane using 1064 nm, 532 nm and 355 nm beams from a Nd:YAG laser. They also obtained C_nH_2 ($n = 8$, 10, 12, 14) after laser ablation of C_{60} in hexane and methanol using 1064 nm, 532 nm, 355 nm and 266 nm beams from a Nd:YAG laser. They suggested that C_2 radicals, produced by ablation, connect continuously with each other to form polyyne and that this growth is terminated by capping with hydrogen atoms at both ends of the polyyne. The average and maximum chain length is determined by the reaction probability in concerted reactions of polymerization and hydrogenation, which strongly depended on the solvent employed. In our case, C_nH_2 ($n = 8$, 10, 12, 14) were obtained but longer $n = 16$ polyynes were not detected.

It was found that there was a threshold fluence below which the polyyne absorption bands were not observed. This indicates that the mechanism resulting in polyyne production is typical of a photothermal laser ablation processes [21,22]. The fluence and irradiation time dependence for the production of polyynes is shown in Fig. 7(b) and (c). It is interesting that the production of polyynes was quenched at longer timescales, which indirectly also suggests that the polyynes may be formed in a photo-thermal process having an activation threshold. This can be rationalized because large particles can absorb many photons in close proximity meaning that the total heating per unit volume is relatively large in the solvent zone surrounding the irradiated particle (the heated volume which should be considered also includes the

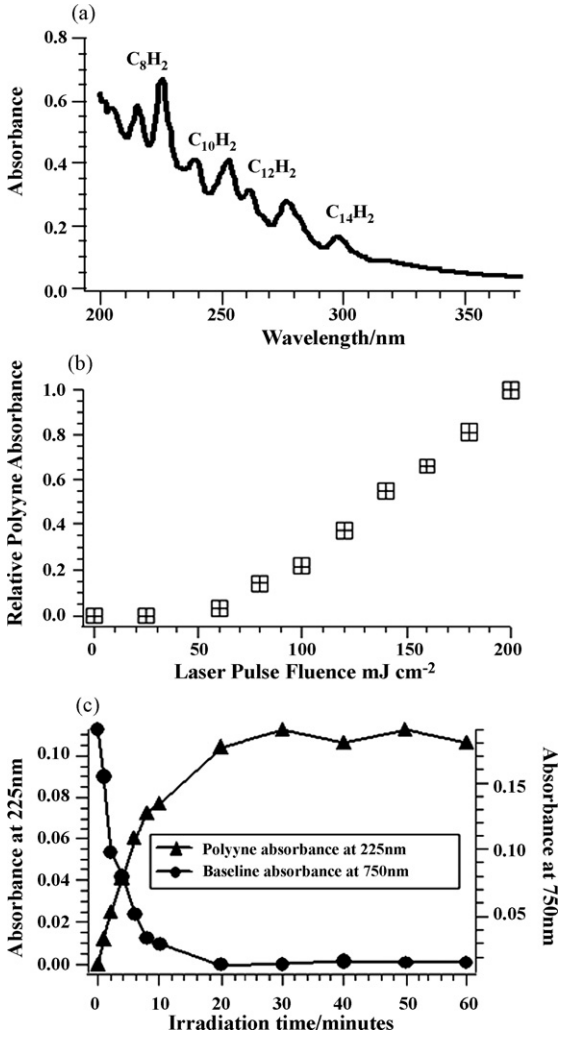

Fig. 7. (a). Absorption spectrum and assignment of polyynes in a filtrate from a suspension laser ablated in ethanol. (b) Fluence dependence for the yield of polyyne determined off-line for a filtered suspension of PTCDA in ethanol, using the magnitude of the absorption peaks for the respective polyynes. (c). Polyene absorbance at 225 nm (filtered sample) as a function of irradiation time compared to the time course for the loss of the baseline (un-filtered sample) at 750 nm due to reduction in light scattering as nano-particles form (pulse fluence of 200 mJ cm^{-2}).

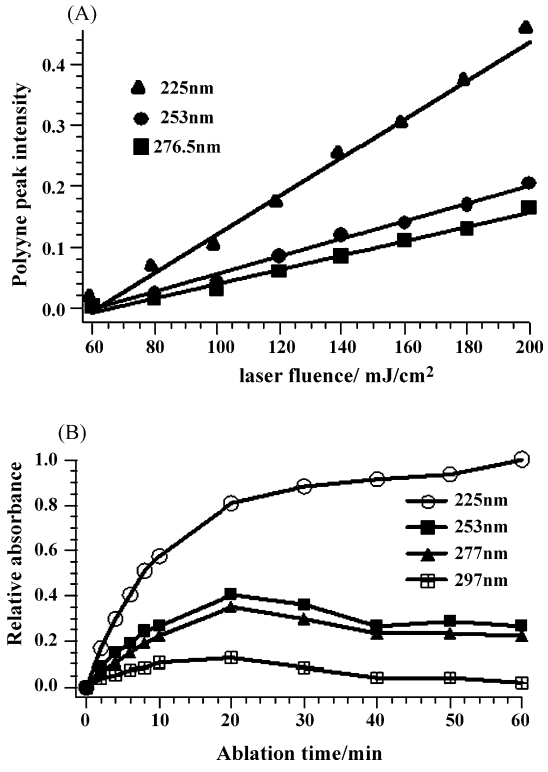

Fig. 8. (a) Fluence dependence of polyyne production after 20 min of irradiation. (b) Time dependence of polyyne production at a fluence of 200 mJ cm^{-2}.

surrounding solvent into which heat can dissipate). However, as smaller and smaller particles form, the resulting heating caused by absorption of the laser pulses becomes more dispersed within the mixed suspension and solvent. This is because the PTCDA itself is in a more dispersed state. The smaller particles will therefore be able to dissipate their heat to the solvent faster and more efficiently than can the larger particles. To test this hypothesis we compared the timescale for polyyne production with that for the reduction in the amount of scattered light, which must follow the reduction in particle size. The amount of light scattering was determined by monitoring the raised baseline absorption at 750 nm. This data is plotted in Fig. 7(c) and clearly shows the direct time correlation for these two processes.

The dependence of the polyyne chain length on the irradiation time and the laser fluence was determined. As shown in Fig. 8a, it was found that the polyyne chain lengths increased approximately linearly with fluence. This implies that the relative production of all polyynes is similar with fluence. As can be seen in Fig. 8b, at longer irradiation times the relative amount of short chain polyyne was slightly favored. The reason for this is not clearly understood, but it implies that the polyynes are themselves subject to secondary reactions after their formation in which they are cut forming shorter chain length final products.

3.4. Emission of perylene formed in the filtrate

The emission and excitation spectra of colorless supernatants, which were obtained by filtration just after ablation had been stopped, were compared to those of perylene, as shown below

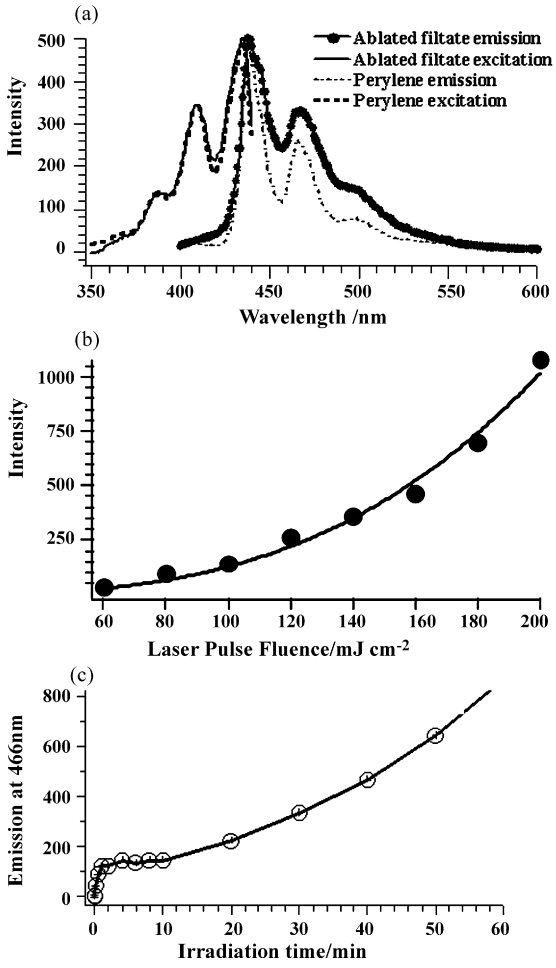

Fig. 9. (a) Excitation and emission spectra of filtrates from ablated suspensions of PTCDA in ethanol compared with those for pure perylene in ethanol. (b) Fluence dependence of perylene yield as determined off-line with the irradiation stopped after 20 min of irradiation, using the intensity of the perylene peak at 466 nm (the same time course was determined for the emission at 438 nm). (c) Perylene yield as a function of laser irradiation time at a pulse fluence of 200 mJ cm^{-2} determined off line with the irradiation stopped after 20 min of irradiation, using the magnitude of the respective perylene peak.

in Fig. 9(a). The filtrate's emission and excitation spectra are identical to the corresponding perylene spectra in terms of the peak positions; however, they differ slightly in terms of peak to valley heights. In view of the peak positions, which were not shifted compared to those of perylene, we suggest that the filtrate of the ablated mixture contains a series of perylene derivatives that are not more conjugated than the parent perylene molecule. However, in view of the difference in the valley height between the peaks, compared to the perylene spectrum, it is possible that there is some inhomogenous line broadening, perhaps because some of the perylene may still have saturated alkyl chains attached in various substitution patterns. The summation of many very similar derivatives, having the same overall conjugation may result in some spectral broadening. Laser ablation is a high energy phenomenon and can result in many uncontrolled side reactions involving radicals and even the solvent.

The detection of perylene or its derivatives is a clear indication that the anhydride side groups can be removed during

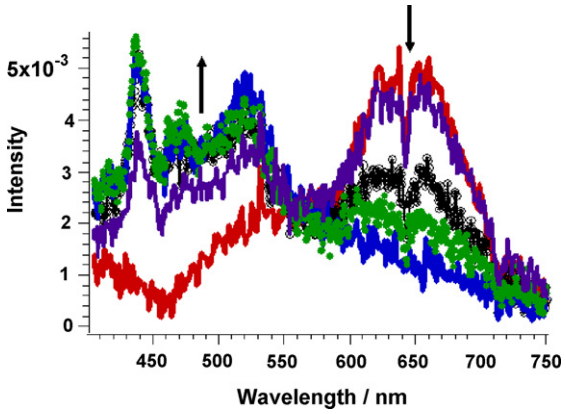

Fig. 10. The shot to shot evolution in the emission spectrum measured in-situ as nanoparticles form with a laser fluence of 200 mJ cm^{-2}. Arrows indicate direction of change during shot by shot accumulated laser pulses for 1, 100, 500, 1000 and 2000 laser shots. Note: this data was measured during single shot by shot evolution (not 10 Hz).

the process of laser ablation, which supports this mechanism as a probable process occurring during pulsed laser deposition of PTCDA reaction products to form PPN as previously assigned [7,8]. The mechanism of the perylene production is partially clarified by examination of the fluence and time dependences of the perylene production. This data is shown in Fig. 9(b) and (c). The perylene production occurs even from low fluences with no threshold. This indicates that it is not a thermally activated process. However, the perylene production increases to the 3rd power of the laser fluence. This indicates that it is a multi-photon and possibly a tri-photonic process with the caveat that a further complicating feature of the process is revealed by monitoring the time dependence of perylene production at higher laser fluences as described in the next paragraph.

In Fig. 9(c) it is apparent that the fastest rate of perylene production was in the first 60 s of irradiation at a repetition rate of 10 Hz. In other words the fastest rate of production was in the first 600 laser shots, at a laser fluence of 200 mJ cm^{-2}. After this time the rate of production dropped drastically, but then increased again at longer timescales. We hypothesize that this must be due to the formation of a layer of decomposed material at the particle surface during the first 600 laser shots, which prevents direct excitation of the PTCDA below this decomposed surface layer. The layer is possibly a high carbon content decomposition product, which can absorb laser light and photothermally react to form polyynes, but does not form perylene photochemically. To test this hypothesis we observed the evolution of emission occurring from an identical stirred suspension of PTCDA in ethanol for every laser shot that was absorbed over 2000 laser shots. This data is shown in Fig. 10. Here the dips observed at around 640 nm are due to a feature of the detector and can be ignored. From this data it is clear that the main emission detected during the first few shots of pulsed laser excitation is from PTCDA itself and is characterized by a peak at ~650 nm from the CT band, which is similar to the emission spectrum shown in Fig. 5(b). However, this emission is nearly totally quenched within 600 laser shots and replaced with a broader emission at shorter wavelength, which probably results from irradiation and ablation of the decomposed particle surface. This later emission spectrum also contains some features due to the excitation of perylene, which became dissolved in the solution during irradiation using the initial 600 laser pulses. Other emitting soluble products that could contribute to the emission spectra obtained after 600 shots did not form. This can be stated because only perylene peaks were observed when the same solution was excited below the ablation threshold at 355 nm, meaning that the broad emission background is the result of multiphotonic ionization and plasma formation during the ablation process and is not due to single photon induced emission from side products. It is clear from this data that, at 10 Hz repetition rate, 600 s would indeed be sufficient time to create an outer layer on the particles, which would absorb most of the 355 nm pulse, preventing excitation of the inner core of PTCDA. Of course some PTCDA would remain exposed especially as the particles became more and more finely divided and the surface area increased. This would result in the observed acceleration of perylene production at even longer timescales, especially since decomposition is expected to occur less and less as the particles divide further and further and as photo-thermal processes become less efficient. We can conclude that the perylene derivatives are produced by the direct excitation of PTCDA in a multi (probably 3) photonic process. Further mechanistic assignment would require a transient time resolved study, which is beyond the scope of the current work.

3.5. Surface temperature of the particles

It is interesting to estimate the surface temperature of the nanoparticles just after the absorption of the laser pulse. To do this we need to know the density, heat capacity and the absorption coefficient of the PTCDA. The absorption coefficient of solid PTCDA at 355 nm can be estimated to be 2.5–8.9 × 10^4/cm [15,36]. The lower value is obtained from the absorbance of an 80 nm thick film of nanoparticles [14], which would have a lower density than the bulk solid. The higher value is for a single crystal and is therefore more representative of a bulk solid [36]. The heat capacity of a typical organic molecular solid at around room temperature can be estimated as around 1 J/gK [37]. However, note that this value will no doubt increase with temperature and especially so if the melting point is exceeded, if indeed the particles have time to melt before the heat generated from the photoexcitation is dissipated. We can assume that the density of PTCDA is approximately 1 g cm^{-3}. The surface temperature rise can then be estimated in the limiting case using the following expression; $\Delta T = I_0\alpha/\rho C_p$ [38]. Where ΔT is the temperature rise, I_0 is the laser fluence in J cm^{-2}, α is the absorption coefficient in cm^{-1}, ρ is the density in g cm^{-3} and C_p is the heat capacity in J/gK. Keeping C_p constant we can estimate that the maximum temperature rise would be 1000 K at 40 mJ cm^{-2} and 5000 K at 200 mJ cm^{-2} if α is 2.5 × 10^4 cm^{-1}. These estimates increase to 3560 K and 17800 K if α is 8.9 × 10^4 cm^{-1}. These are maximum values because the melting point and probably even the boiling point could be exceeded at these temperatures and because the value of C_p would surely increase with temperature. Further, the heat would begin to dissipate during the laser pulse. Dissipation of this heat would inevitably lead to heating of the

bulk solvent especially considering that the laser repetition rate is 10 Hz. If each pulse contains 100 mJ (the maximum case for 200 mJ cm^{-2}) then, at 10 Hz, 60 J would be absorbed by the system every minute since the pulse is completely absorbed. In the case of water this would lead to a temperature rise of 1.4 K/min. However, losses to the surroundings would limit the maximum temperature rise to a steady state value lower than product of the heating rate and time as the system is not insulated. In the case of ethanol the maximum heating rate would be 3 K/min, again the total temperature rise would be limited by heat loss to the surroundings.

4. Conclusion

Irradiation of suspensions of PTCDA in water or ethanol using the 3rd harmonic of a Nd:YAG laser resulted in the formation of PTCDA nanoparticles. No nanoparticle production was seen when irradiation was carried out in cyclohexane or toluene. The production of nanoparticles was accompanied by the formation of polyynes in a photo-thermal process and perylene in a multi-photonic process. A reduction in the amount of these side products is possible by forming the nanoparticles at lower laser fluences. This method of dispersion of insoluble compounds as nano-aggregates using laser ablation could also have application for the delivery of insoluble or sparingly soluble pharmaceutically important compounds, such as drugs or compounds used in chemo and photodynamic therapies. The possibility that a particle's surface can be modified by photochemical and photothermal processes is also revealed.

Acknowledgements

This research was supported by Grant-in-Aid for Scientific Researches from the Ministry of Education, Culture, Sports, Science and Technology (No. 13440204 and 17034060). A part of this work was carried out at the Venture Business Laboratory of Tohoku University.

References

[1] S.R. Forrest, Chem. Rev. 97 (1997) 1793.
[2] J.G. Xue, S.R. Forrest, Phys. Rev. B 69 (2004) 245322.
[3] J.L. Bredas, R.H. Baughman, J. Chem. Phys. 83 (1985) 1316.
[4] (a) K. Tanaka, S. Yamanaka, K. Ueda, S. Takeda, T. Yamabe, Synth. Met. 20 (1987) 333;
(b) M. Murakami, S. Iijima, S. Yoshimura, J. Appl. Phys. 60 (1986) 3856.
[5] M. Yudasaka, Y. Tasaka, M. Tanaka, H. Kamo, Y. Ohki, S. Usami, S. Yoshimura, Appl. Phys. Lett. 64 (1994) 3237.
[6] H. Kamo, M. Yudasaka, S. Kurita, T. Matsui, R. Kikuchi, Y. Ohki, S. Yoshimura, Synth. Met. 68 (1994) 61.
[7] S. Nishio, R. Mase, T. Oba, A. Matsuzaki, H. Sato, Appl. Surf. Sci. 127–129 (1998) 589.
[8] S. Nishio, H. Sato, T. Yamabe, Appl. Phys. A 69 (1999) S711.
[9] A. Ouchi, A. Yabe, Jpn. J. Appl. Phys. 31 (1992) L1295.
[10] K. Kamiya, T. Noda, M. Ide, J. Tanaka, Synth. Met. 71 (1995) 1765.
[11] P.J. Unwin, D. Onoufriou, T.S. Jones, Surf. Sci. 547 (2003) 45.
[12] A.Y. Kobitski, R. Scholz, D.R.T. Zahn, H.P. Wagner, Phys. Rev. B 68 (2003) 155201.
[13] A. Nollau, M. Hoffmann, T. Fritz, K. Leo, Thin Solid Films 368 (2000) 130.
[14] R. Scholz, A.Y. Kobitski, T.U. Kampen, M. Schreiber, D.R.T. Zahn, G. Jungnikel, M. Elstner, M. Sternberg, T. Frauenheim, Phys. Rev. B 20 (61) (2000) 13659.
[15] V. Bulovic, P.E. Burrows, S.R. Forrest, J.A. Cronin, M.E. Thompson, Chem. Phys. 210 (1996) 1.
[16] A.B. Djurisic, C.Y. Kwong, W.L. Guo, Z.T. Liu, H.S. Kwok, W.K. Chan, Appl. Phys. A 77 (2003) 649.
[17] H. Katagi, H. Kasai, S. Okada, H. Oikawa, K. Komatsu, H. Matsuda, Z. Liu, H. Nakanishi, Jpn. J. Appl. Phys. 35 (1996) L1364.
[18] A. Masuhara, S. Ohhashi, H. Kasai, S. Okada, H. Oikawa, H. Nakanishi, J. Nonliear Opt. Phys. Mater. 13 (3–4) (2004) 587.
[19] V.V. Volkov, T. Asahi, H. Masuhara, A. Masuhara, H. Kasai, H. Oikawa, H. Nakanishi, J. Phys. Chem. B 108 (23) (2004) 7674.
[20] A. Masuhara, H. Kasai, S. Okada, H. Oikawa, M. Terauchi, M. Tanaka, H. Nakanishi, Jpn. J. Appl. Phys. II Lett. 40 (10B) (2001) L1129.
[21] S. Link, C. Burda, B. Nikoobankht, M.A. El-Sayed, J. Phys. Chem. B 104 (2000) 6152.
[22] F. Mafune, J. Kohno, Y. Takeda, T. Kondow, J. Phys. Chem. B 105 (2001) 5114.
[23] T. Tsuji, K. Iryo, Y. Nishimura, M. Tsuji, J. Photochem. Photobiol-A 145 (2001) 201.
[24] C. Liang, T. Sasaki, T. Shimizu, N. Koshizaki, Chem. Phys. Lett. 145 (2004) 58.
[25] M. Sugiyama, H. Okazaki, S. Koda, Jpn. J. Appl. Phys. 41 (2002) 4666.
[26] A. Pyatenko, K. Shimokawa, M. Yamaguchi, O. Nishimura, M. Suzuki, Appl. Phys. A 79 (4–6) (2004) 803.
[27] Y. Tamaki, T. Asahi, H. Masuhara, Appl. Surf. Sci. 168 (2000) 85.
[28] Y. Tamaki, T. Asahi, H. Masuhara, J. Phys. Chem. A 106 (2002) 2135.
[29] Y. Tamaki, T. Asahi, H. Masuhara, Jpn. J. Appl. Phys. 42 (2003) 2725.
[30] M. Tsuji, T. Tsuji, S. Kuboyama, S.H. Yoon, Y. Korai, T. Tsujimoto, K. Kubo, A. Mori, I. Mochida, Chem. Phys. Lett. 355 (2002) 101.
[31] M. Tsuji, S. Kuboyama, T. Matsuzaki, T. Tsuji, Carbon 41 (2003) 2148.
[32] S. Nishio, C. Kanezawa, H. Fukumura, Appl. Phys. A. 79 (2004) 1449.
[33] R. Eastmond, T.R. Johnson, D.R.M. Walton, Tetrahedron 28 (1972) 4601.
[34] A.J. Ferguson, T.S. Jones, J. Phys. Chem. B 110 (2006) 6891.
[35] A. Pyatenko, M. Yamaguchi, M. Suzuki, J. Phys. Chem. B 109 (2005) 21608.
[36] M.I. Alonso, M. Garriga, N. Karl, J.O. Osso, F. Schreiber, Org. Electron. (2002) 23.
[37] N. Sallime, J.M. Shaw, Fluid Phase Equilib. 237 (2005) 100.
[38] J. Hobley, S. Nishio, K. Hatanaka, H. Fukumura, in: H.S. Nalwa (Ed.), Handbook of Photochemistry and Photobiology, 2, American Scientific Publishers, Los Angeles, USA, 2003, ISBN 1-58883-023-3, p. 262.